

Extended s -wave pairing from an emergent Feshbach resonance in bilayer nickelate superconductors

Pietro Borchia,^{1,2} Hannah Lange,^{1,3,4} and Fabian Grusdt^{1,4}

¹Ludwig-Maximilians-University Munich, Theresienstr. 37, Munich D-80333, Germany

²Technical University of Munich, TUM School of Natural Sciences, Physics Department, 85748 Garching, Germany

³Max-Planck-Institute for Quantum Optics, Hans-Kopfermann-Str.1, Garching D-85748, Germany

⁴Munich Center for Quantum Science and Technology, Schellingstr. 4, Munich D-80799, Germany

(Dated: February 20, 2025)

Since the discovery of unconventional superconductivity in cuprates, unraveling the pairing mechanism of charge carriers in doped antiferromagnets has been a long-standing challenge. Motivated by the discovery of high- T_c superconductivity in nickelate bilayer $\text{La}_3\text{Ni}_2\text{O}_7$ (LNO), we study a minimal mixed dimensional (MixD) $t - J$ model supplemented with a repulsive Coulomb interaction V . When hole-doped, previous numerical simulations revealed that the system exhibits strong binding energies, with a phenomenology resembling a BCS-to-BEC crossover accompanied by a Feshbach resonance between two distinct types of charge carriers. Here, we perform a mean-field analysis that enables a direct observation of the BCS-to-BEC crossover as well as microscopic insights into the crossover region and the pairing symmetry for two-dimensional bilayers. We benchmark our mean-field description by comparing it to density-matrix renormalization group (DMRG) simulations in quasi-one dimensional settings and find remarkably good agreement. For the two-dimensional system relevant to LNO our mean-field calculations predict a BCS pairing gap with an extended s -wave symmetry, directly resulting from the pairing mechanism's Feshbach-origin. Our analysis hence gives insights into pairing in unconventional superconductors and, further, can be tested in currently available ultracold atom experiments.

Starting with the discovery of superconductivity in cuprate materials about four decades ago [1–4], the search for superconductors with high critical temperatures has revealed unconventional superconductivity in various materials, including nickelate and cuprate compounds [5, 6]. Recently, the bilayer nickelate $\text{La}_3\text{Ni}_2\text{O}_7$ (LNO) was observed to become superconducting under pressure at a critical temperature of 80K [7–9], with a pairing gap of extended s -wave symmetry predicted by theoretical works [10–13], similar to those in infinite layer nickelates [14], iron-based superconductors [15], and the strongly coupled bilayer Hubbard model [16–18]. Following the observation of high- T_c superconductivity in LNO, theoretical studies suggested that a minimal effective low-energy model that governs the physics of these materials is a mixed dimensional (MixD) bilayer $t - J$ model, i.e., a single band $t - J$ model with suppressed inter-layer hopping but strong antiferromagnetic coupling between the layers (see Fig. 1) [19–22]. More realistic multi-orbital models have also been proposed [21, 23, 24]. In order to find a minimal description for nickelate superconductors, investigating the pairing mechanism in MixD $t - J$ bilayers represents a crucial step toward developing a microscopic understanding of pairing in these unconventional superconductors. However, the nature of pairing and the pairing symmetry within this model remain elusive.

In contrast to conventional superconductors, high- T_c superconductors feature significant pairing gaps, i.e. smaller Cooper pairs which possibly experience repulsive Coulomb interactions, the Coulomb repulsion V is typically not negligible in these materials [25]. We account for that with an additional nearest neighbor repulsion V between holes on the same rung of the bilayer.

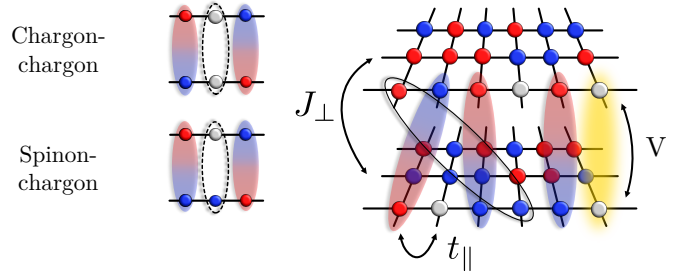


FIG. 1. Schematic depiction of the 2D MixD+V bilayer model (right) and its quasi-particle constituents (left). We highlight the emergent constituents that characterize the two sides of the BCS-to-BEC crossover existing in this system: on the BCS side the system is dominated by spatially extended pairs (sc^2) of spinon-chargeons (sc 's), involving one extended singlet (highlighted in the figure). The BEC side features tightly bound chargon-chargeons (cc 's) characterized by the Coulomb repulsion V (yellow shadow).

These MixD+V systems have been shown to host the following emergent structures upon doping the ground state at half-filling, consisting of singlets on each rung of the ladder [25–30]: (i) at small V/J_{\perp} two holes form a tightly bound state of two chargons (chargon(c)-chargon(c) pair, cc 's) with strong binding energy. This is the result of inter-layer exchange J_{\perp} and coherent movement of the cc 's through the system in order to minimize distortions of the (antiferromagnetic) AFM background [27]. (ii) At large V/J_{\perp} the system is dominated by spatially extended pairs of two partons, a spinon and a chargon (spinon(s)-chargon(c) pair, sc 's). In between (i) and (ii) a crossover from a Bose-Einstein condensate (BEC) of

cc 's to a strongly correlated Bardeen–Cooper–Schrieffer (BCS) regime with pairs of sc 's (sc^2) is observed [23, 25], which features a pairing dome with relatively high binding energy [30]. Each sc^2 is thus composed of two mesons (sc 's), comprising a total of four partons: two chargons and two spinons.

While binding between holes in the cc 's can be explained with kinetic arguments, making it favorable for holes to move together through the system [26, 27], binding of pairs of sc 's into sc^2 originates from a more subtle mechanism, leading to more spatially extended Cooper pairs of holes [25, 30]: in the BCS regime, where sc 's govern the low energy physics, numerical and analytical results suggest that binding is mediated via couplings to the high energy cc channel, resembling a Feshbach resonance between the low energy (“open”) sc channel and the high energy (“closed”) cc channel. This Feshbach mediated pairing mechanism [31, 32] features many similarities to the phenomenology of bilayer nickelate but also cuprate superconductors [25, 29, 30]: (i) Pairing is facilitated by doping, leading to a dome of binding energies with its peak at intermediate doping; (ii) Pairing only requires short-range antiferromagnetic (AFM) correlations but no long-range magnetic order; (iii) The Fermi surface volume changes [24], similar to the small-to-large Fermi surface transition in cuprates; (iv) For single layer models, the resulting pairing gap is predicted to have the d -wave symmetry observed in cuprates [31], and, as we will show here, for bilayers the extended s -wave symmetry predicted for LNO can be explained. So far, these observations have been made by comparing effective theories in terms of the emergent constituents and numerical observations in single and coupled ladders deep in the cc 's and sc^2 regimes. However, a description of the intermediate regime where sc^2 and cc hybridize, needed to fully test the prediction of Feshbach mediated pairing, is lacking.

Here, we go beyond earlier analysis and derive an effective mean-field description of the sc and cc constituents in the intermediate regime, that captures the essential physics of the BCS-to-BEC crossover and of the Feshbach resonance. We compare our mean-field predictions to density matrix renormalization group (DMRG) simulations of the MixD+V ladder to validate the model. Then, we extend our analysis to the 2D systems relevant to LNO. Our analysis allows to understand the BCS-to-BEC crossover in terms of the corresponding order parameters. Furthermore, it reveals the extended s -wave symmetry of the pairing gap as a direct consequence of the Feshbach mediated pairing mechanism, see Fig. 2.

I. MICROSCOPIC MODEL

The MixD $t - J$ bilayer supplemented with a repulsive interaction V was first introduced in [23, 25, 30]. It features nearest neighbor hopping with amplitude t_{\parallel} ,

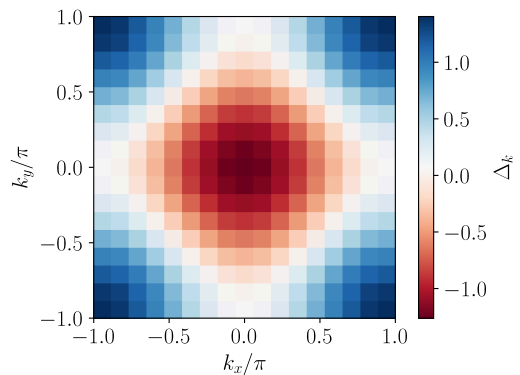


FIG. 2. In the crossover regime, the spinon-chargon pairs are described by the BCS wavefunction. Here we consider a 2D MixD+V model on a 16×16 square lattice with $\frac{t_{\parallel}}{V} = 0.1$, $J_{\perp} = V$ and $N_h = 12$ holes in the system. The figure shows the value of the BCS order parameter Δ_k realizing an extended s -wave pairing symmetry.

superexchange interaction J_{\perp} and repulsive Coulomb interaction V between holes on the same rung, i.e.

$$\hat{\mathcal{H}} = -t_{\parallel} \hat{\mathcal{P}} \sum_j \sum_{\mu, \sigma} \left(\hat{c}_{j+1\mu\sigma}^{\dagger} \hat{c}_{j\mu\sigma} + \text{h.c.} \right) \hat{\mathcal{P}} + J_{\perp} \sum_j \left(\hat{\mathbf{S}}_{j0} \cdot \hat{\mathbf{S}}_{j1} - \frac{1}{4} \hat{n}_{j0} \hat{n}_{j1} \right) + V \sum_j \hat{n}_{j0}^h \hat{n}_{j1}^h \quad (1)$$

Here, $\hat{\mathcal{P}}$ is the Gutzwiller projector onto the subspace with maximum single occupancy per site. Spin and density operators at site j and layer $\mu = 0, 1$ are represented by $\hat{\mathbf{S}}_{j\mu}$ and $\hat{n}_{j\mu} = \hat{n}_{j\mu\uparrow} + \hat{n}_{j\mu\downarrow}$. The hole density operators are denoted by $\hat{n}_{j\mu}^h = 1 - \hat{n}_{j\mu}$.

The motivation for studying the MixD+V model is twofold: firstly, the recently discovered bilayer nickelate $\text{La}_3\text{Ni}_2\text{O}_7$, showing superconducting behavior with $T_c = 80\text{K}$ under high pressure, effectively realizes a bilayer MixD $t - J$ model. This can be seen from DFT calculations that reveal that the low energy degrees of freedom are the $3d_{z^2}$ and $3d_{x^2-y^2}$ Ni orbitals [20], featuring strong Hund’s coupling between them. The d_{z^2} orbitals induce interlayer AFM superexchange interactions via the O-2p orbitals in the intercalated LaO layer. In contrast, the $d_{x^2-y^2}$ orbitals are responsible for a weak intralayer hopping t_{\parallel} and AFM coupling J_{\parallel} . In the limit of large Hund’s coupling between the two $3d$ orbitals, the system realizes an effective AFM interaction J_{\perp} between the two layers, and the interlayer hopping t_{\perp} is suppressed [20]. Moreover, as stated before, we need to account for the Coulomb repulsion V between neighboring holes, arising from the limited spatial extension of Cooper pairs in unconventional superconductors. The second motivation to study the mixD+V model is their realizability in cold atom experiments: in Ref. [28], a mixD ladder was realized by applying a potential offset between the legs of the ladder, effectively enhancing J_{\perp} and suppressing the perpendicular hopping [26–28].

This system can be supplemented with nearest-neighbor repulsion by doping one leg with doublons and one with holes, see Refs. [25, 30, 33].

The ground state of this MixD+V model at zero doping consists of one singlet on each rung of the ladder [26, 27]. At finite doping, the physics of the system is determined by the competition between the kinetic energy of the holes and the energy from the distortion of the magnetic background due to the motion of the holes. In the tight-binding regime $t_{\parallel} \ll J_{\perp}, V$ the emerging constituents can be easily understood in the following two limits: when $J_{\perp} \gg V$, the low-energy constituents of the system are cc 's, minimizing the distortion of the spin background. On the contrary, for $J_{\perp} \ll V$, each rung will tend to be occupied at maximum by one hole (and one spin), forming a spinon-chargeon. In this regime, both emergent charge carriers can be assumed point-like, i.e., with constituents on the same rung [25, 27]. In previous works [25, 30], it was shown that the transition between the two limits can be explained as a crossover associated with a Feshbach resonance from tightly bound pairs of holes (closed channel) at small repulsion to more spatially extended, correlated pairs of individual holes (open channel) at large repulsion [31]. In this picture, attractive interactions in the open channel are mediated by processes that couple to the closed channel even for large repulsion $V > J_{\perp}, t_{\parallel}$.

II. MEAN-FIELD THEORY

Earlier studies [25, 30] provided a qualitative understanding of the physics of the MixD+V model in the limiting cases where either sc 's (large V/J_{\perp}) or cc 's (small V/J_{\perp}) are dominant in the system, but the exploration of the crossover regime $J_{\perp} \simeq V$ was limited to DMRG simulations of single and a few coupled ladders. Furthermore, such numerical methods do not directly provide access to the pairing gap. In contrast, here we obtain microscopic insight into the physics of the MixD+V model in the crossover regime where both cc 's and sc 's are present: we derive an effective two-channel Hamiltonian in terms of sc 's $f_{j\mu\sigma}^{(\dagger)}$ and cc 's $b_j^{(\dagger)}$ by performing a Schrieffer-Wolff transformation of Eq.(1) assuming

$$t_{\parallel} \ll J_{\perp}, V \quad (2)$$

hence point-like sc 's and cc 's. Then, we develop a mean-field theory (MF) to solve the resulting model.

In this limit, both sc 's and cc 's belong to the low-energy manifold, whereas the high-energy subspace contains configurations comprised of distorted singlets. The effective Hamiltonian we obtain reads

$$\begin{aligned} \hat{\mathcal{H}}_{\text{eff}}^{sc,cc} &= \hat{\mathcal{H}}_{\text{kin}}^{sc} + \hat{\mathcal{H}}_{\text{pot}}^{sc} + \hat{\mathcal{H}}_{\text{pot}}^{cc} + \hat{\mathcal{H}}_{\text{int}}^{sc,sc} + \hat{\mathcal{H}}_{\text{rec}}^{sc,cc} \quad (3) \\ &+ \mu_h(\hat{N}_f + \hat{N}_b - N_h) \end{aligned}$$

$$\begin{aligned} \hat{\mathcal{H}}_{\text{kin}}^{sc} &= +\frac{t_{\parallel}}{2} \sum_{\langle i,j \rangle} \sum_{\mu\sigma} \hat{\mathcal{P}}_f \left(\hat{f}_{i\mu\sigma}^{\dagger} \hat{f}_{j\mu\sigma} + h.c. \right) \hat{\mathcal{P}}_f \quad (4) \\ &- t_{\parallel} \sum_{\langle i,j \rangle} \sum_{\mu\sigma} \hat{\mathcal{P}}_f \left(\hat{f}_{i\mu\sigma}^{\dagger} \hat{b}_j^{\dagger} \hat{b}_i \hat{f}_{j\mu\sigma} + h.c. \right) \hat{\mathcal{P}}_f \end{aligned}$$

$$\hat{\mathcal{H}}_{\text{pot}}^{sc} = \left(J_{\perp} - \frac{3}{2} \frac{t_{\parallel}^2}{J_{\perp}} \right) \sum_{j\mu} \hat{n}_{j\mu}^f \quad (5)$$

$$\hat{\mathcal{H}}_{\text{pot}}^{cc} = (V + J_{\perp}) \sum_i \hat{b}_i^{\dagger} \hat{b}_i \quad (6)$$

$$\begin{aligned} \hat{\mathcal{H}}_{\text{int}}^{sc,sc} &= +\frac{3}{2} \frac{t_{\parallel}^2}{J_{\perp}} \sum_{\langle i,j \rangle} \sum_{\mu\mu'} \hat{n}_{i\mu}^f \hat{n}_{j\mu'}^f \quad (7) \\ &- 4 \frac{t_{\parallel}^2}{V} \sum_{\langle i,j \rangle} \left(-\hat{\mathbf{J}}_i \cdot \hat{\mathbf{J}}_j + \frac{1}{4} \right) \left(\hat{\mathbf{S}}_i \cdot \hat{\mathbf{S}}_j + \frac{3}{4} \hat{n}_i^f \hat{n}_j^f \right) \end{aligned}$$

$$\hat{\mathcal{H}}_{\text{rec}}^{sc,cc} = -\frac{t_{\parallel}}{\sqrt{2}} \sum_{\langle i,j \rangle} \sum_{\mu,\sigma} (-1)^{\sigma} \hat{\mathcal{P}}_f \left(\hat{f}_{i\mu\sigma}^{\dagger} \hat{f}_{j\bar{\mu}\bar{\sigma}}^{\dagger} \hat{b}_j + h.c. \right) \hat{\mathcal{P}}_f \quad (8)$$

where Eq.(4) corresponds to the kinetic energy of the sc 's and cc 's, and Eq.(5, 6) are respectively the terms associated with the sc 's and the cc 's chemical potential. The term in Eq.(7) takes into account the interactions between sc 's sitting on neighboring rungs, which are subject to repulsive interaction $\propto \frac{3}{2} \frac{t_{\parallel}^2}{J_{\perp}}$ and attractive interaction $\propto \frac{t_{\parallel}^2}{V}$ for triplet states. The term in Eq.(8) describes the recombination of a pair of two neighboring sc 's (open channel) into one cc 's (closed channel) and vice versa giving rise to the Feshbach resonance as the presence of cc 's lowers the energy of the sc channel. The last term $\propto \mu_h$ fixes the total number of holes in the system. In the above, $\hat{n}_{j\mu}^f = \hat{n}_{j\mu\uparrow}^f + \hat{n}_{j\mu\downarrow}^f$ denotes the sc 's density while the layer-isospin operator $\hat{\mathbf{J}}_i$ and the spin operator $\hat{\mathbf{S}}_i$ are defined in Appendix A.

In order to capture the low-energy physics of $(sc)^2$ -to- cc crossover we consider the following ansatz for the ground state wavefunction

$$\begin{aligned} |\Psi\rangle &= \left[\prod_k \left(u_k + v_k \frac{1}{\sqrt{2}} \sum_{\sigma} (-1)^{\sigma} \hat{f}_{k\mu\sigma}^{\dagger} \hat{f}_{-k\bar{\mu}\bar{\sigma}}^{\dagger} \right) \right. \\ &\left. \otimes \mathcal{N} \exp(\beta \hat{b}_{k=0}^{\dagger}) \right] |0\rangle \quad (9) \end{aligned}$$

where the first term accounts for the BCS pairing of sc 's with variational parameters $u_k, v_k \in \mathbb{C}$. The explicit singlet structure of the sc 's (note that $\bar{\sigma}$ and $\bar{\mu}$ denote the respective opposite spin and layer) is motivated by the fact that for sufficiently large V holes on the same rung strongly repel each other due to Coulomb interaction. Therefore as $\frac{J_{\perp}}{V}$ is decreased, the cc 's are

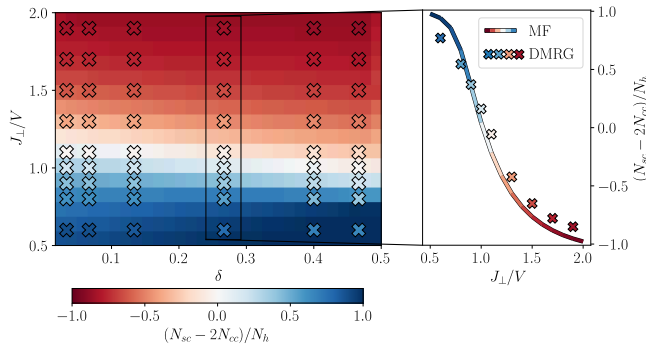


FIG. 3. We compare the sc and cc densities for a 1D ladder as the ratio $\frac{J_{\perp}}{V}$ and the doping δ are tuned. We compute $(N_{sc} - 2N_{cc})/N_h$ where N_{sc} and N_{cc} are respectively the number of sc 's and cc 's in the system as defined in Sec. III; N_h is the total number of holes. This allows to distinguish the two sides of the crossover. The inset shows the section at constant doping $\delta = \frac{8}{30}$ with the corresponding colors. We find good agreement between DMRG (crosses) and mean-field (color-plot/solid line) for a MixD+V ladder of size $L = 30$ where we have fixed $\frac{t_{\parallel}}{V} = 0.1$.

disrupted and the displacement of the two holes constituting the cc leads to the formation of a tilted singlet between two neighbouring spinons on opposite layers. The second term describes the BEC of tightly bound cc 's with normalization constant \mathcal{N} and order parameter $\beta \in \mathbb{C}$. Here, $|0\rangle$ denotes the sc 's and cc 's vacuum state, consisting of singlets on each rung. Our goal in the following is to tune $\frac{J_{\perp}}{V}$ to transition from the BEC regime of tightly bound cc 's, where we expect large β , to the BCS regime where the sc 's form extended Cooper pairs in a BCS state. At the resonance, between the two regimes, the effective sc scattering length diverges. To describe this intermediate regime, it is important to include explicitly the coupling between the two channels (sc and cc).

By minimizing the energy expectation value of the Hamiltonian in Eq.(3) with respect to the variational parameters of the wavefunction in Eq.(9), $\partial_{u_k v_k} \partial_{\beta} \langle \Psi | \hat{\mathcal{H}}_{\text{eff}}^{sc,cc} | \Psi \rangle = 0$, see Appendix B, we obtain the ground state properties of the system. In order to analytically perform the mean-field calculations we neglect the Gutzwiller projections in Eq.(3). This is expected to be a good approximation for low doping and we restrict our analysis to values of the hole doping $\delta < 0.5$.

III. BENCHMARKING MEAN-FIELD IN 1D MIXD+V LADDERS

We compare the results from our mean-field analysis with DMRG simulations, obtained using the package SyTen with particle conservation in each leg and a global

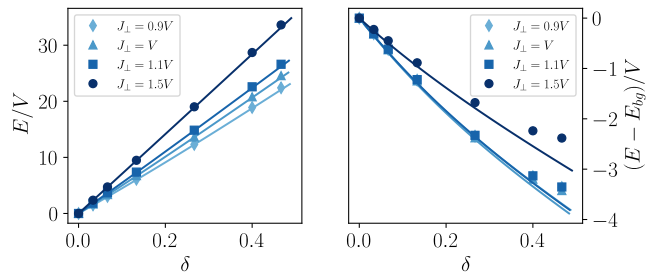


FIG. 4. The ground state energy E (left) of the microscopic model for a 1D ladder system from DMRG (markers) is reproduced well by the mean-field prediction for the effective Hamiltonian (solid lines). The agreement is good also for the ground state energies without considering the contribution from the background distortion $E - E_{bg} = E - J_{\perp}N_{sc} - (V + J_{\perp})N_{cc}$ (right). Here, we consider different values of $\frac{J_{\perp}}{V}$ through the crossover for a MixD+V ladder of size $L = 30$, where $\frac{t_{\parallel}}{V} = 0.1$ is fixed.

$U(1)_{S_z}$ symmetry [34, 35]. In Fig. 3 we focus on 1D ladder systems where the sc 's and cc 's densities of the microscopic model of Eq.(1) computed with DMRG are compared to the ground state mean-field results obtained from the effective Hamiltonian in Eq.(3). In particular, the difference between the number of holes contributing to the sc 's sector and cc 's sector $\propto N_{sc} - 2N_{cc}$ is shown as a function of $\frac{J_{\perp}}{V}$ and hole doping δ . The two different regimes can be identified by the change in sign of the above quantity. Here, $\hat{n}_{cc} = \frac{1}{L} \sum_i \hat{n}_{i\mu=1}^h \hat{n}_{i\mu=0}^h$ and $\hat{n}_{sc} = \frac{1}{L} \sum_i \hat{n}_{i\mu=1}^h (1 - \hat{n}_{i\mu=0}^h)$ for the microscopic model, and $\hat{n}_{cc} = \frac{1}{L} \sum_i \hat{b}_i^{\dagger} \hat{b}_i$ and $\hat{n}_{sc} = \frac{1}{L} \sum_{i\mu} \hat{n}_{i\mu}^f$ for the mean-field (MF) theory. As for the MF calculations, both species are considered to be point-like since the system is probed in the tight binding regime $t_{\parallel} \ll J_{\perp}, V$. We find that for $V > J_{\perp}$ the system is dominated by sc 's and the number of cc 's is negligible. For lower doping however, it is expected to grow linearly for $\delta > 0.5$ due to the single occupancy restriction [25], which we cannot capture within MF theory. For $V < J_{\perp}$ the formation of sc 's is suppressed and the holes are bound together in cc 's.

Fig. 4 (left) compares the ground state energy obtained from DMRG and MF theory for different values of $\frac{J_{\perp}}{V}$ at low doping. In the tight binding regime, when the system is hole doped, a large contribution to the ground state energy comes from the distortion of the AFM background: $J_{\perp}N_{sc}$ for the sc 's and $(V + J_{\perp})N_{cc}$ for the cc 's. However, the role of the kinetic, interaction, and recombination terms is not negligible; this is shown in Fig. 4 (right) where we compare the ground state energies after subtracting the sc 's and cc 's background terms mentioned above. In both cases, there is good agreement, validating our MF approach.

Next, we calculate the binding energies, defined as

$$E_B(N_h) = 2(E_{N_h-2} - E_{N_h-1}) - (E_{N_h-2} - E_{N_h}) \quad (10)$$

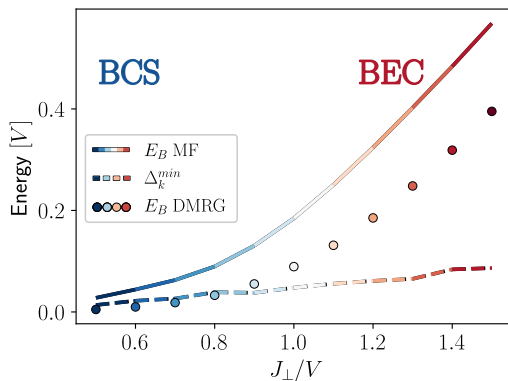


FIG. 5. The binding energies E_B computed for a 1D ladder system via DMRG (markers) is compared to mean-field theory (solid line) as J_\perp is tuned. Here, we also show the value of the order parameter Δ_k at the minimum of E_k , i.e. where the band gap is minimal (dashed line). We consider a ladder system of size $L = 30$ with fixed doping $\delta = \frac{14}{30}$ and $\frac{t_\parallel}{V} = 0.1$.

where N_h is the number of holes in the system, added alternately to each layer. The expression can be evaluated directly from the DMRG ground state energies at different doping. For the mean-field theory, we obtain the binding energy by computing the terms in Eq. (10) separately. We consider the system in the BEC regime; here, the addition of two holes leads to the formation of a cc and $E_{N_h-2} - E_{N_h} \approx 0$ since the energy required to add a quasi-particle to the condensate is approximately zero. However, the addition of one single hole corresponds to the creation of a single quasi-particle in the BCS state which leads to an energy variation of $E_{N_h-1} - E_{N_h} = \min_k(E_k)$ with $E_k = \sqrt{\Delta_k^2 + \xi_k^2}$ where Δ_k is the BCS order parameter and ξ_k is the dispersion relation for sc 's, see Appendix B. Therefore the binding energies are given by $E_B = 2(E_{N_h-2} - E_{N_h-1}) - (E_{N_h-2} - E_{N_h}) \approx 2(\min_k(E_k)) - 0 = 2 \min_k(E_k)$, which corresponds to the pairing gap obtained by diagonalizing the BCS mean-field Hamiltonian, see Appendix C. As shown in Fig. 5 we find that as $\frac{J_\perp}{V}$ increases, the binding energy E_B becomes larger, in agreement with the picture of tightly bound pairs of holes [27, 28]. The values obtained from the mean-field calculations qualitatively follow the results from DMRG simulations.

Another indication that the system undergoes a BCS-to-BEC crossover is obtained by comparing the binding energy E_B of the fermion pairs with the order parameter Δ_k evaluated at k^* where the band gap is minimal $\Delta_k^{\min} = \Delta_k(k^*)$ where $k^* = \arg \min(E_k)$. This accounts for the phase coherence between the pairs: in the BCS region of extended pairs the two quantities converge since pairs form and develop phase coherence at the same energy, whereas they are significantly different in the BEC regime, where fermions pair up with binding energy E_B but the condensation energy is lower [36, 37]. This is a hallmark of the BCS-to-BEC crossover.

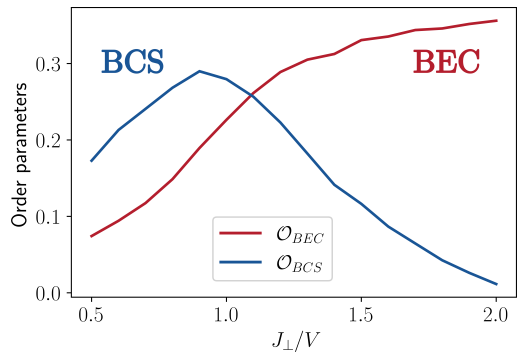


FIG. 6. We show the order parameters for the BEC and BCS regimes of the ansatz wavefunction in a 1D ladder system, as defined in the main text. Here we consider a ladder of size $L = 30$ at fixed doping $\delta = \frac{8}{30}$ and fixed $\frac{t_\parallel}{V} = 0.1$.

Furthermore, the mean-field description provides direct access to the order parameters characterizing the BEC and BCS regimes. A key requirement for these order parameters is that they remain well-defined in the thermodynamic limit, $L \rightarrow \infty$. To this end, we define

$$\mathcal{O}_{BEC} = \sqrt{\frac{N_{cc}}{L^d}}, \quad (11)$$

$$\mathcal{O}_{BCS} = \frac{1}{L^d} \sum_k \frac{|\Delta_k|}{\sqrt{\Delta_k^2 + \xi_k^2}} \quad (12)$$

$$\xrightarrow{L \rightarrow \infty} \frac{1}{(2\pi)^d} \int_{\text{BZ}} d^d k \frac{|\Delta_k|}{\sqrt{\Delta_k^2 + \xi_k^2}},$$

which correspond to the BEC and BCS order parameters, respectively, for a d -dimensional system. The summation over the Brillouin zone (BZ) ensures that the order parameter is defined without resolving individual momentum states in k -space. In Fig. 6 we analyze a 1D ladder system $d = 1$. This analysis confirms our picture of a BCS-to-BEC crossover around $\frac{J_\perp}{V} \approx 1.2$.

IV. EXTENDED S-WAVE PAIRING IN 2D MIXD+V MODELS

In the previous section, we compared the mean-field predictions for different observables with the DMRG simulations of the microscopic model in 1D. This showed that the MixD+V ladder under consideration realizes a BCS-to-BEC crossover as $\frac{J_\perp}{V}$ and δ are tuned. Now, the mean-field calculations can be easily extended to the case of 2D bilayer systems and provide access to the pairing gap. Indeed, the sc 's in the system pair up in singlets on opposite layers and are effectively described by the BCS wavefunction in Eq. (9), which is characterized by the parameter Δ_k , defined in Appendix B. As shown in Fig. 2, the pairing function associated with the $(sc)^2$ in a bilayer square lattice system features an extended s -wave

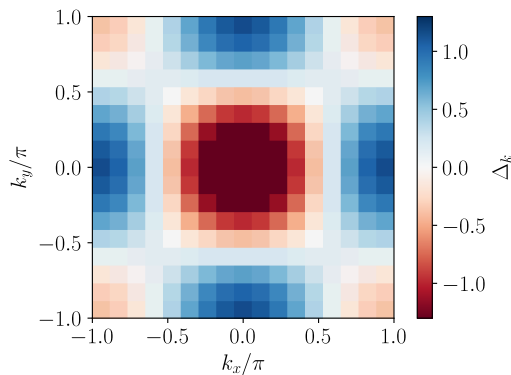


FIG. 7. The pairing gap Δ_k is modified by the introduction of diagonal recombinations of sc 's and cc 's and an additional region with opposite sign appears at the corners of the Brillouin zone. Here we consider a 2D MixD+V model on a 16×16 square lattice with $\frac{t_{\parallel}}{V} = 0.1$, $J_{\perp} = V$, $N_h = 12$ holes in the system, and with $\epsilon = 1.5$.

symmetry, i.e. it presents a symmetric non trivial momentum dependence with a clear nodal region and sign inversion.

This prediction is particularly intriguing in the light of the results from Ref. [11] where Cooper pairing with s_{\pm} -wave symmetry was found using functional renormalization group techniques. The pairing gap that we obtain in our mean-field analysis has a simple structure and shows only two distinct areas in the Brillouin zone with different sign. We argue that this is due to the assumption of point-like sc 's and cc 's which is valid in the tight binding regime $t_{\parallel} \ll V, J_{\perp}$. However, additional features of the pairing gap are expected to appear when considering the internal structure of the constituents which becomes relevant for larger t_{\parallel} . Specifically, allowing recombination of sc 's and cc 's along the diagonal directions of the lattice, leads to the formation of a third region at the corners of the Brillouin zone, see Fig. 7. The diagonal recombination is implemented in the Hamiltonian of Eq. (3) by introducing the term

$$\hat{\mathcal{H}}_{\text{diag rec}}^{sc,cc} = -\epsilon \frac{t_{\parallel}}{\sqrt{2}} \sum_{i,j} \sum_{\mu,\sigma} (-1)^{\sigma} \hat{\mathcal{P}}_f (f_{i\mu\sigma}^{\dagger} f_{j\bar{\mu}\bar{\sigma}}^{\dagger} \hat{b}_j + h.c.) \hat{\mathcal{P}}_f \quad (13)$$

where ϵ tunes the strength of the interaction between the two channels along the i, j diagonal neighbors.

V. CONCLUSION

In conclusion, we have explored the physics of the MixD+V bilayer system and its implications for high- T_c superconductivity in the bilayer nickelate $\text{La}_3\text{Ni}_2\text{O}_7$ (LNO). Previous work [20–23, 25, 27, 30] identified two different regimes upon hole doping the effective low energy model of these materials: on one side, the BCS region of spatially extended sc 's Cooper pairs, and on the other, the BEC region of tightly bound cc 's. Additionally, our numerical analysis indicates that in the BCS limit, pairing between sc 's arises from a Feshbach resonance, in analogy with atomic physics. However, a microscopic understanding of the intermediate regime was lacking. In this study, starting from the microscopic model, we derived an effective Hamiltonian in terms of the sc 's and cc 's, and proposed an ansatz ground state wavefunction to capture the essential physics of the charge carriers across the BCS-to-BEC crossover. The formulation of the mean-field theory allowed us to gain a microscopic understanding of the system by constructing a clear conceptual framework where the emergent constituents and their interactions could be investigated. By comparison with DMRG simulations in ladder systems we have demonstrated the validity of the model and showed that it effectively describes the low energy physics of the system. Notably, the main result of this work is the prediction of a pairing gap with extended s -wave symmetry in the bilayer model, which characterizes the $(sc)^2$ Cooper pairs. Our finding paves the way to explore even more complex scenarios by considering the internal structure of the charge carriers, which we propose will lead to additional features in the pairing gap, see Fig. 7. Lastly, we remark that the MixD+V bilayer system can be studied using ultracold atom experiments by a modification of the setup in Ref. [28], incorporating nearest-neighbor repulsion [25].

VI. ACKNOWLEDGMENTS

We would like to thank Annabelle Bohrdt, Lukas Homeier, Henning Schlömer and Matjaz Kebric for helpful discussions. We acknowledge funding by the Deutsche Forschungsgemeinschaft (DFG, German Research Foundation) under Germany's Excellence Strategy – EXC-2111 – 390814868 and from the European Research Council (ERC) under the European Union's Horizon 2020 research and innovation program (Grant Agreement no 948141) — ERC Starting Grant SimUcQuam. HL acknowledges support by the International Max Planck Research School.

[1] J. G. Bednorz and K. A. Müller, Possible high- T_c superconductivity in the balacuo system, *Zeitschrift für Physik*

B Condensed Matter **64**, 189 (1986).

- [2] P. A. Lee, N. Nagaosa, and X.-G. Wen, Doping a mott insulator: Physics of high-temperature superconductivity, *Rev. Mod. Phys.* **78**, 17 (2006).
- [3] D. J. Scalapino, Superconductivity and spin fluctuations, *Journal of Low Temperature Physics* **117**, 179 (1999).
- [4] P. Nozières and S. Schmitt-Rink, Bose condensation in an attractive fermion gas: From weak to strong coupling superconductivity, *Journal of Low Temperature Physics* **59**, 195 (1985).
- [5] A. Schilling, M. Cantoni, J. D. Guo, and H. R. Ott, Superconductivity above 130 k in the hg-ba-ca-cu-o system, *Nature* **363**, 56 (1993).
- [6] D. Li, K. Lee, B. Y. Wang, M. Osada, S. Crossley, H. R. Lee, Y. Cui, Y. Hikita, and H. Y. Hwang, Superconductivity in an infinite-layer nickelate, *Nature* **572**, 624 (2019).
- [7] H. Sun, M. Huo, X. Hu, J. Li, Z. Liu, Y. Han, L. Tang, Z. Mao, P. Yang, B. Wang, J. Cheng, D.-X. Yao, G.-M. Zhang, and M. Wang, Signatures of superconductivity near 80 K in a nickelate under high pressure, *Nature* **621**, 493 (2023).
- [8] Y. Zhang, D. Su, Y. Huang, H. Sun, M. Huo, Z. Shan, K. Ye, Z. Yang, R. Li, M. Smidman, M. Wang, L. Jiao, and H. Yuan, High-temperature superconductivity with zero-resistance and strange metal behavior in $\text{La}_3\text{Ni}_2\text{O}_7$ (2023), arXiv:2307.14819.
- [9] J. Hou, P. T. Yang, Z. Y. Liu, J. Y. Li, P. F. Shan, L. Ma, G. Wang, N. N. Wang, H. Z. Guo, J. P. Sun, Y. Uwatoko, M. Wang, G. M. Zhang, B. S. Wang, and J. G. Cheng, Emergence of high-temperature superconducting phase in the pressurized $\text{La}_3\text{Ni}_2\text{O}_7$ crystals (2023), arXiv:2307.09865.
- [10] Y. Zhang, L.-F. Lin, A. Moreo, T. A. Maier, and E. Dagotto, Electronic structure, magnetic correlations, and superconducting pairing in the reduced ruddlesden-popper bilayer $\text{La}_3\text{Ni}_2\text{O}_6$ under pressure: Different role of $d_{3z^2-r^2}$ orbital compared with $\text{La}_3\text{Ni}_2\text{O}_7$, *Phys. Rev. B* **109**, 045151 (2024).
- [11] Q.-G. Yang, D. Wang, and Q.-H. Wang, Possible s_{\pm} -wave superconductivity in $\text{La}_3\text{Ni}_2\text{O}_7$, *Phys. Rev. B* **108**, L140505 (2023).
- [12] Y.-B. Liu, J.-W. Mei, F. Ye, W.-Q. Chen, and F. Yang, s^{\pm} -wave pairing and the destructive role of apical-oxygen deficiencies in $\text{La}_3\text{Ni}_2\text{O}_7$ under pressure, *Phys. Rev. Lett.* **131**, 236002 (2023).
- [13] H. Sakakibara, N. Kitamine, M. Ochi, and K. Kuroki, Possible high T_c superconductivity in $\text{La}_3\text{Ni}_2\text{O}_7$ under high pressure through manifestation of a nearly half-filled bilayer hubbard model, *Phys. Rev. Lett.* **132**, 106002 (2024).
- [14] A. Kreisel, B. M. Andersen, A. T. Rømer, I. M. Eremin, and F. Lechermann, Superconducting instabilities in strongly correlated infinite-layer nickelates, *Phys. Rev. Lett.* **129**, 077002 (2022).
- [15] A. V. Chubukov, Pairing mechanism in fe-based superconductors (2011), arXiv:1110.0052 [cond-mat.supr-con].
- [16] H. Zhai, F. Wang, and D.-H. Lee, Antiferromagnetically driven electronic correlations in iron pnictides and cuprates, *Phys. Rev. B* **80**, 064517 (2009).
- [17] T. A. Maier and D. J. Scalapino, Pair structure and the pairing interaction in a bilayer hubbard model for unconventional superconductivity, *Phys. Rev. B* **84**, 180513 (2011).
- [18] M. Nakata, D. Ogura, H. Usui, and K. Kuroki, Finite-energy spin fluctuations as a pairing glue in systems with coexisting electron and hole bands, *Phys. Rev. B* **95**, 214509 (2017).
- [19] Z. Luo, X. Hu, M. Wang, W. Wú, and D.-X. Yao, Bilayer Two-Orbital Model of $\text{La}_3\text{Ni}_2\text{O}_7$ under Pressure, *Phys. Rev. Lett.* **131**, 126001 (2023).
- [20] C. Lu, Z. Pan, F. Yang, and C. Wu, Interlayer-Coupling-Driven High-Temperature Superconductivity in $\text{La}_3\text{Ni}_2\text{O}_7$ under Pressure, *Phys. Rev. Lett.* **132**, 146002 (2024).
- [21] H. Oh and Y.-H. Zhang, Type-ii $t-j$ model and shared superexchange coupling from hund's rule in superconducting $\text{La}_3\text{Ni}_2\text{O}_7$, *Phys. Rev. B* **108**, 174511 (2023).
- [22] X.-Z. Qu, D.-W. Qu, J. Chen, C. Wu, F. Yang, W. Li, and G. Su, Bilayer $t-J-J_{\perp}$ model and magnetically mediated pairing in the pressurized nickelate $\text{La}_3\text{Ni}_2\text{O}_7$ (2024).
- [23] H. Yang, H. Oh, and Y.-H. Zhang, Strong pairing from a small fermi surface beyond weak coupling: Application to $\text{La}_3\text{Ni}_2\text{O}_7$, *Phys. Rev. B* **110**, 104517 (2024).
- [24] H. Yang, H. Oh, and Y.-H. Zhang, Strong pairing and symmetric pseudogap metal in double kondo lattice model: from nickelate superconductor to tetralayer optical lattice (2024), arXiv:2408.01493 [cond-mat.str-el].
- [25] H. Lange, L. Homeier, E. Demler, U. Schollwöck, F. Grusdt, and A. Bohrdt, Feshbach resonance in a strongly repulsive ladder of mixed dimensionality: A possible scenario for bilayer nickelate superconductors, *Phys. Rev. B* **109**, 045127 (2024).
- [26] A. Bohrdt, L. Homeier, C. Reinmoser, E. Demler, and F. Grusdt, Exploration of doped quantum magnets with ultracold atoms, *Ann. Phys.* **435**, 168651 (2021).
- [27] A. Bohrdt, L. Homeier, I. Bloch, E. Demler, and F. Grusdt, Strong pairing in mixed-dimensional bilayer antiferromagnetic Mott insulators, *Nat. Phys.* **18**, 651 (2022).
- [28] S. Hirthe, T. Chalopin, D. Bourgund, P. Bojović, A. Bohrdt, E. Demler, F. Grusdt, I. Bloch, and T. A. Hilker, Magnetically mediated hole pairing in fermionic ladders of ultracold atoms, *Nature* **613**, 463 (2023).
- [29] H. Schlömer, U. Schollwöck, F. Grusdt, and A. Bohrdt, Superconductivity in the pressurized nickelate $\text{La}_3\text{Ni}_2\text{O}_7$ in the vicinity of a bec-bcs crossover (2023), arXiv:2311.03349 [cond-mat.str-el].
- [30] H. Lange, L. Homeier, E. Demler, U. Schollwöck, A. Bohrdt, and F. Grusdt, Pairing dome from an emergent Feshbach resonance in a strongly repulsive bilayer model, *Phys. Rev. B* **110**, L081113 (2024).
- [31] L. Homeier, H. Lange, E. Demler, A. Bohrdt, and F. Grusdt, Feshbach hypothesis of high- t_c superconductivity in cuprates, *Nature Communications* **16**, <https://doi.org/10.1038/s41467-024-55549-4> (2025).
- [32] V. Crépel and L. Fu, New mechanism and exact theory of superconductivity from strong repulsive interaction, *Science Advances* **7**, eabh2233 (2021), <https://www.science.org/doi/pdf/10.1126/sciadv.abh2233>.
- [33] H. Schlömer, H. Lange, T. Franz, T. Chalopin, P. Bojović, S. Wang, I. Bloch, T. A. Hilker, F. Grusdt, and A. Bohrdt, Local control and mixed dimensions: Exploring high-temperature superconductivity in optical lattices (2024), arXiv:2406.02551 [cond-mat.quant-gas].
- [34] C. Hubig, Symmetry-protected tensor networks, Ludwig-Maximilians-Universität München (2017).

- [35] C. Hubig, N. L. F. Lachenmaier, L. S. T. Reinhard, A. Swoboda, and M. Grundner, "the syten toolkit" ().
- [36] C. A. R. Sá de Melo, M. Randeria, and J. R. Engelbrecht, Crossover from BCS to Bose superconductivity: Transition temperature and time-dependent Ginzburg-Landau theory, *Phys. Rev. Lett.* **71**, 3202 (1993).
- [37] C. A. R. Sá de Melo, When fermions become bosons: Pairing in ultracold gases, *Phys. Today* **61**, 45 (2008).
- [38] M. M. Parish, The BCS–BEC crossover, in *Cold Atoms* (Imperial College Press, 2014) pp. 179–197.
- [39] C. Hubig, F. Lachenmaier, N.-O. Linden, T. Reinhard, L. Stenzel, A. Swoboda, and M. Grundner, The SYTEN toolkit., <https://syten.eu> ().
- [40] C. Hubig, Symmetry-protected tensor networks, <https://edoc.ub.uni-muenchen.de/21348/> (2017).
- [41] H. Schlömer, A. Bohrdt, L. Pollet, U. Schollwöck, and F. Grusdt, Robust stripes in the mixed-dimensional $t-j$ model, *Phys. Rev. Res.* **5**, L022027 (2023).

Appendix A: Derivation of the effective Hamiltonian

In this section, we derive the effective Hamiltonian describing the system in terms of spinon-chargons (sc) and chargon-chargons (cc); subsequently, we show how to obtain the ground-state wavefunction parameters through the variational method. Our study focuses on the intermediate regime in the crossover region where $t_{\parallel} \ll J_{\perp} \simeq V$. In order to derive the effective spinon-chargon and chargon-chargon Hamiltonian from the microscopic MixD Hamiltonian, we perform Schrieffer-Wolff transformations.

Here, we use the notation introduced previously for the spinon-chargon and chargon-chargon annihilation (creation) operators: $f_{j\mu\sigma}^{(\dagger)}$ and $b_j^{(\dagger)}$ [25]

$$\hat{f}_{i\mu\sigma}^{\dagger} |\dots 0 \dots\rangle = \left| \dots \overset{\sigma}{\circ} \dots \right\rangle \quad (\text{A1})$$

$$\hat{f}_{i\mu\sigma} \left| \dots \overset{\sigma}{\circ} \dots \right\rangle = |\dots 0 \dots\rangle \quad (\text{A2})$$

with $\mu \in \{0, 1\}$ denoting the leg degree of freedom of the spinon-chargon, and

$$\hat{b}_i^{\dagger} |\dots 0 \dots\rangle = \left| \dots \overset{\circ}{\circ} \dots \right\rangle \quad (\text{A3})$$

$$\hat{b}_i \left| \dots \overset{\circ}{\circ} \dots \right\rangle = |\dots 0 \dots\rangle \quad (\text{A4})$$

where singlets are identified by \circ , chargon-chargon pairs by $\overset{\circ}{\circ}$ and where $\overset{\sigma}{\circ}$ and $\overset{\circ}{\sigma}$ denote spinon-chargon pairs in the upper and lower layer, respectively. The sc-cc vacuum consists of singlets on each rung, represented by $|\dots \circ \dots\rangle$. Isolated spinon-chargons allow low-energy (Gutwiller projected) hopping processes [25]

$$\hat{\mathcal{H}}_{sc}^{(1)} = -\frac{t_{\parallel}}{2} \sum_{\langle i,j \rangle} \sum_{\mu\sigma} \hat{\mathcal{P}}_f \left(\hat{f}_{i\mu\sigma}^{\dagger} \hat{f}_{j\mu\sigma} + h.c. \right) \hat{\mathcal{P}}_f \quad (\text{A5})$$

In this regime, recombination processes involving chargon-chargon and spinon-chargon pairs remain in the low-energy channel

$$\hat{\mathcal{H}}_{cc,sc}^{(1)} = -\frac{t_{\parallel}}{\sqrt{2}} \sum_{\langle i,j \rangle} \sum_{\mu\sigma} (-1)^{\sigma} \left(\hat{f}_{i\mu\sigma}^{\dagger} \hat{f}_{j\bar{\mu}\bar{\sigma}}^{\dagger} \hat{b}_j + h.c. \right) \quad (\text{A6})$$

For isolated spinon-chargons, we also have to consider second-order processes due to recombination with the high-energy channel of tilted singlets, which have an amplitude of $-2\frac{3}{4}\frac{t_{\parallel}^2}{J_{\perp}}$ where the factor of 2 comes from the two directions in which the particles can hop [25]. Moreover, each spinon-chargon contributes $+J_{\perp}$ for every broken singlet w.r.t. the sc-cc vacuum. Together it gives

$$\hat{\mathcal{H}}_{sc}^{(2)} = \left(J_{\perp} - \frac{3}{2} \frac{t_{\parallel}^2}{J_{\perp}} \right) \sum_{j\mu} \hat{n}_{j\mu}^f \quad (\text{A7})$$

If two spinon-chargons occupy neighboring rungs, second-order recombination in each other's direction is obstructed, and we need to take that into account by introducing the additional term

$$+\frac{3}{2} \frac{t_{\parallel}^2}{J_{\perp}} \sum_{\langle i,j \rangle} \sum_{\mu\mu'} \hat{n}_{i\mu}^f \hat{n}_{j\mu'}^f \quad (\text{A8})$$

When spinon-chargons and chargon-chargons are located on neighboring rungs, they can exchange position by the first-order hopping process of one particle

$$\hat{\mathcal{H}}_{sc,cc}^{(1)} = -t_{\parallel} \sum_{\langle i,j \rangle} \sum_{\mu\sigma} \left(\hat{f}_{i\mu\sigma}^{\dagger} \hat{b}_j^{\dagger} \hat{b}_i \hat{f}_{j\mu\sigma} + h.c. \right) \quad (\text{A9})$$

Neighboring spinon-chargons can recombine via the high-energy triplet channel V in a second-order process

$$\hat{\mathcal{H}}_{\text{triplet}} = 2 \frac{t_{\parallel}^2}{V} \sum_{\langle i,j \rangle} \left(J_i^+ J_j^- + J_i^- J_j^+ + 2 J_i^z J_j^z - \frac{1}{2} \right) \left(\hat{\mathbf{S}}_i \cdot \hat{\mathbf{S}}_j + \frac{3}{4} \hat{n}_i^f \hat{n}_j^f \right) \quad (\text{A10})$$

$$= -4 \frac{t_{\parallel}^2}{V} \sum_{\langle i,j \rangle} \left(-\hat{\mathbf{J}}_i \cdot \hat{\mathbf{J}}_j + \frac{1}{4} \right) \left(\hat{\mathbf{S}}_i \cdot \hat{\mathbf{S}}_j + \frac{3}{4} \hat{n}_i^f \hat{n}_j^f \right) \quad (\text{A11})$$

where $\hat{\mathbf{J}}_i = \frac{1}{2} \sum_{\sigma} \sum_{\mu\mu'} \hat{f}_{i\mu\sigma}^{\dagger} \boldsymbol{\sigma}_{\mu\mu'} \hat{f}_{i\mu'\sigma}$ is the layer isospin operator and $\hat{P}_T = \left(\hat{\mathbf{S}}_i \cdot \hat{\mathbf{S}}_j + \frac{3}{4} \hat{n}_i^f \hat{n}_j^f \right)$ is the projector onto the triplet state with $\hat{\mathbf{S}}_i = \frac{1}{2} \sum_{\mu} \sum_{\sigma\sigma'} \hat{f}_{i\mu\sigma}^{\dagger} \boldsymbol{\sigma}_{\sigma\sigma'} \hat{f}_{i\mu\sigma}$. The singlet channel lies in the low-energy manifold and has already been included in Eq. (A6). Lastly, we need to include the energy for the chargon-chargons in the system with respect to the vacuum state: for each cc, we have a broken singlet, which contributes $+J_{\perp}$ and the on-rung interaction V

$$(V + J_{\perp}) \sum_i \hat{b}_i^{\dagger} \hat{b}_i \quad (\text{A12})$$

The full-perturbative Hamiltonian is

$$\begin{aligned} \hat{\mathcal{H}}_{\text{eff}}^{sc,cc} = & -\frac{t_{\parallel}}{\sqrt{2}} \sum_{\langle i,j \rangle} \sum_{\mu\sigma} (-1)^{\sigma} \hat{\mathcal{P}}_f \left(\hat{f}_{i\mu\sigma}^{\dagger} \hat{f}_{j\bar{\mu}\bar{\sigma}}^{\dagger} \hat{b}_j + h.c. \right) \hat{\mathcal{P}}_f + \frac{t_{\parallel}}{2} \sum_{\langle i,j \rangle} \sum_{\mu\sigma} \hat{\mathcal{P}}_f \left(\hat{f}_{i\mu\sigma}^{\dagger} \hat{f}_{j\mu\sigma} + h.c. \right) \hat{\mathcal{P}}_f \\ & - t_{\parallel} \sum_{\langle i,j \rangle} \sum_{\mu\sigma} \hat{\mathcal{P}}_f \left(\hat{f}_{i\mu\sigma}^{\dagger} \hat{b}_j^{\dagger} \hat{b}_j \hat{f}_{j\mu\sigma} + h.c. \right) \hat{\mathcal{P}}_f + \left(J_{\perp} - \frac{3}{2} \frac{t_{\parallel}^2}{J_{\perp}} \right) \sum_{j\mu} \hat{n}_{j\mu}^f + \frac{3}{2} \frac{t_{\parallel}^2}{J_{\perp}} \sum_{\langle i,j \rangle} \sum_{\mu\mu'} \hat{n}_{i\mu}^f \hat{n}_{j\mu'}^f \\ & - 4 \frac{t_{\parallel}^2}{V} \sum_{\langle i,j \rangle} \left(-\hat{\mathbf{J}}_i \cdot \hat{\mathbf{J}}_j + \frac{1}{4} \right) \left(\hat{\mathbf{S}}_i \cdot \hat{\mathbf{S}}_j + \frac{3}{4} \hat{n}_i^f \hat{n}_j^f \right) + (V + J_{\perp}) \sum_i \hat{b}_i^{\dagger} \hat{b}_i \\ & + \mu_h \left(\sum_j \sum_{\mu\sigma} \hat{n}_{j\mu\sigma}^f + 2 \sum_j \hat{n}_j^b - N_h \right) \end{aligned} \quad (\text{A13})$$

with the last term, we have introduced the chemical potential μ_h , which controls the number of holes N_h in the system. Now, to derive an analytical expression for $\langle \hat{H} \rangle$, we consider the Hamiltonian in momentum space by performing the Fourier transform $\hat{f}_{j\mu\sigma}^{\dagger} = \frac{1}{\sqrt{L}} \sum_k \hat{f}_{k\mu\sigma}^{\dagger} e^{-ikj}$ and $\hat{b}_j^{\dagger} = \frac{1}{\sqrt{L}} \sum_k \hat{b}_k^{\dagger} e^{-ikj}$ where we have a 1-dimensional system of size L . This gives us

$$\begin{aligned} \hat{\mathcal{H}}_{\text{eff},k}^{sc,cc} = & -\frac{t_{\parallel}}{\sqrt{L}} \sqrt{2} \sum_{kq} \sum_{\mu\sigma} (-1)^{\sigma} \left(\hat{f}_{k\mu\sigma}^{\dagger} \hat{f}_{q-k\bar{\mu}\bar{\sigma}}^{\dagger} \hat{b}_q \cos(k) + h.c. \right) + t_{\parallel} \sum_k \sum_{\mu\sigma} \cos(k) \hat{f}_{k\mu\sigma}^{\dagger} \hat{f}_{k\mu\sigma} \\ & - 2 \frac{t_{\parallel}}{L} \sum_{kk'q} \sum_{\mu\sigma} \cos(q) \hat{f}_{k\mu\sigma}^{\dagger} \hat{b}_{k'}^{\dagger} \hat{b}_{k'+q} \hat{f}_{k'-q\mu\sigma} + \left(J_{\perp} - \frac{3}{2} \frac{t_{\parallel}^2}{J_{\perp}} \right) \sum_{k\mu} \hat{n}_{k\mu}^f \\ & + \frac{3}{2} \frac{t_{\parallel}^2}{J_{\perp} L} \sum_{kk'q} \sum_{\substack{\mu\mu' \\ \sigma\sigma'}} \hat{f}_{k\mu\sigma}^{\dagger} \hat{f}_{k'\mu'\sigma'}^{\dagger} \hat{f}_{k'-q\mu'\sigma'} \hat{f}_{k+q\mu\sigma} e^{-iq} \\ & - \frac{t_{\parallel}^2}{VL} \sum_{kk'q} \sum_{\substack{\mu\mu' \\ \sigma\sigma'}} \hat{f}_{k\mu\sigma}^{\dagger} \hat{f}_{k'\bar{\mu}\bar{\sigma}}^{\dagger} \hat{f}_{k'-q\mu'\sigma'} \hat{f}_{k+q\bar{\mu}'\bar{\sigma}'} e^{-iq} + (V + J_{\perp}) \sum_k \hat{b}_k^{\dagger} \hat{b}_k \\ & + \mu_h \left(\sum_k \sum_{\mu\sigma} \hat{f}_{k\mu\sigma}^{\dagger} \hat{f}_{k\mu\sigma} + 2 \sum_k \hat{b}_k^{\dagger} \hat{b}_k - N_h \right) \end{aligned} \quad (\text{A14})$$

where we have neglected the Gutwiller projections, which is an acceptable approximation in the low-doping regime $\delta < 0.5$ where the overlap between different spinon-chargons singlets is negligible.

Appendix B: Derivation of the ground state parameters

The mean-field theory that we provide is based upon an ansatz wavefunction which captures the essential nature of the crossover: the tensor product between the BCS wavefunction where the Cooper pairs are formed by two spinon-

chargons on opposite layers in a spin singlet state and the coherent state of chargon-chargeons at zero quasi-momentum

$$|\Psi\rangle = \left[\underbrace{\prod_k \left(u_k + v_k \frac{1}{\sqrt{2}} \sum_{\sigma} (-1)^{\sigma} \hat{f}_{k1\sigma}^{\dagger} \hat{f}_{-k0\bar{\sigma}}^{\dagger} \right)}_{\text{sc BCS}} \otimes \underbrace{\mathcal{N} \exp(\beta \hat{b}_{k=0}^{\dagger})}_{\text{cc BEC}} \right] |0\rangle \quad (\text{B1})$$

where the first term represents the BCS nature of spinon-chargeons singlets with $u_k, v_k \in \mathbb{C}$ parameters. The second part describes the BEC-like chargon-chargeon regime with normalization constant \mathcal{N} and order parameter $\beta \in \mathbb{C}$. The normalization requirement for the BCS term yields

$$\prod_k (|u_k|^2 + |v_k|^2) \stackrel{!}{=} 1 \quad (\text{B2})$$

which is certainly satisfied if we demand $|u_k|^2 + |v_k|^2 = 1 \forall k$. The ground-state values of the parameters can be determined variationally by minimizing the expected value of the energy $\nabla \langle \Psi | \hat{H} | \Psi \rangle \stackrel{!}{=} 0$. Hence, firstly, we compute the contribution to $\langle \hat{H} \rangle$ for each term in the Hamiltonian. We give an example: consider the second term in Eq.(A14). This term acts trivially on the BEC part of the wavefunction, and so we focus on the following expression

$$\langle 0 | \prod_p \left(u_p^* + v_p^* \frac{1}{\sqrt{2}} \sum_s (-1)^s \hat{f}_{-p0\bar{s}'} \hat{f}_{p1s} \right) \hat{f}_{k\mu\sigma}^{\dagger} \hat{f}_{k\mu\sigma} \prod_{p'} \left(u_{p'} + v_{p'} \frac{1}{\sqrt{2}} \sum_{s'} (-1)^{s'} \hat{f}_{p'1s'}^{\dagger} \hat{f}_{-p'0\bar{s}'} \right) | 0 \rangle \quad (\text{B3})$$

A special role is played by the terms $p = p' = k$ for which we have

$$\langle 0 | \left(u_k^* + v_k^* \frac{1}{\sqrt{2}} \sum_s (-1)^s \hat{f}_{-k0\bar{s}} \hat{f}_{k1s} \right) \hat{f}_{k\mu\sigma}^{\dagger} \hat{f}_{k\mu\sigma} \left(u_k + v_k \frac{1}{\sqrt{2}} \sum_{s'} (-1)^{s'} \hat{f}_{k1s'}^{\dagger} \hat{f}_{-k0\bar{s}'} \right) | 0 \rangle \quad (\text{B4})$$

where the terms contributing are the ones that ensure that the spinon-chargeons are first created and then annihilated. If we consider the case $\mu = 1$ and $\sigma = \uparrow$ the only non-zero contribution is

$$\langle 0 | \frac{1}{2} \overbrace{|v_k|^2 \hat{f}_{-k0\downarrow} \hat{f}_{k1\uparrow} \hat{f}_{k1\uparrow}^{\dagger} \hat{f}_{k1\uparrow} \hat{f}_{k1\uparrow}^{\dagger} \hat{f}_{k1\uparrow} \hat{f}_{-k0\downarrow}^{\dagger}} | 0 \rangle \quad (\text{B5})$$

The same applies for $\mu = 1$ and $\sigma = \downarrow$. The procedure is analogous in the case of $\mu = 0$, but now, we must consider the terms $p = p' = -k$. Hence, taking into account the four possible combinations of μ and σ , we obtain the total contribution for the second term in the Hamiltonian

$$\langle \Psi | t_{\parallel} \sum_{k\mu\sigma} \cos(k) \hat{f}_{k\mu\sigma}^{\dagger} \hat{f}_{k\mu\sigma} | \Psi \rangle = t_{\parallel} \sum_k (|v_k|^2 + |v_{-k}|^2) \cos(k) \quad (\text{B6})$$

The same procedure can be used to determine the contribution from the other terms in the Hamiltonian from Eq.(A14). The total expectation value for the energy is

$$\begin{aligned} \langle \hat{H} \rangle &= -2 \frac{t_{\parallel}}{\sqrt{L}} \sum_k (v_k^* u_k \beta \cos(k) + v_{-k}^* u_{-k} \beta \cos(k) + \text{c.c.}) \\ &+ (t_{\parallel} - 2 \frac{t_{\parallel}}{L} |\beta|^2) \sum_k (|v_k|^2 + |v_{-k}|^2) \cos(k) + \left(J_{\perp} - \frac{3}{2} \frac{t_{\parallel}^2}{J_{\perp}} + \mu_h \right) \sum_k (|v_k|^2 + |v_{-k}|^2) \\ &+ \frac{3}{2} \frac{t_{\parallel}^2}{J_{\perp} L} \sum_{kk'} \left[2 \cos(k - k') (v_k^* u_k u_{k'}^* v_{k'}) + \right. \\ &\quad \left. + |v_k|^2 |v_{k'}|^2 + |v_{-k}|^2 |v_{-k'}|^2 + |v_{-k}|^2 |v_{k'}|^2 + |v_k|^2 |v_{-k'}|^2 \right] \\ &+ (V + J_{\perp} + 2\mu_h) |\beta|^2 - \mu_h N_h \end{aligned} \quad (\text{B7})$$

So far, we haven't made any assumptions on v_k and u_k except for the normalization requirement. However, since $\langle \hat{H} \rangle$ has to be real, we can choose w.l.o.g. $v_k, u_k \in \mathbb{R}$, which we will assume from now on. The terms of fourth order in v_k

in Eq.(B7) correspond to the lowest order mean-field Hartree terms, which can be neglected since they vanish in the limit of short-range interactions [38]. Then Eq.(B7) simplifies to

$$\begin{aligned}
\langle \hat{H} \rangle &= -4 \frac{t_{\parallel}}{\sqrt{L}} \sum_k (v_k u_k \beta \cos(k) + \text{c.c}) \\
&\quad + 2(t_{\parallel} - 2 \frac{t_{\parallel}}{L} |\beta|^2) \sum_k \cos(k) |v_k|^2 + 2 \left(J_{\perp} - \frac{3}{2} \frac{t_{\parallel}^2}{J_{\perp}} + \mu_h \right) \sum_k |v_k|^2 \\
&\quad + 3 \frac{t_{\parallel}^2}{J_{\perp} L} \sum_{kk'} \cos(k - k') (v_k u_k u_{k'} v_{k'}) + (V + J_{\perp} + 2\mu_h) |\beta|^2 - \mu_h N_h
\end{aligned} \tag{B8}$$

In order to determine the ground state properties of the system, we need to minimize $\langle \hat{H} \rangle$. We can exploit the normalization restriction from Eq. (B2) to parametrize the BCS coefficients as $v_k = \sin \frac{\theta_k}{2}$ and $u_k = \cos \frac{\theta_k}{2}$, then

$$\begin{aligned}
\langle \hat{H} \rangle &= -2 \frac{t_{\parallel}}{\sqrt{L}} \sum_k \left[\sin \theta_k \beta \cos(k) + \text{c.c} \right] + \left(2t_{\parallel} - 4 \frac{t_{\parallel}}{L} |\beta|^2 \right) \sum_k \sin^2 \frac{\theta_k}{2} \cos(k) \\
&\quad + 2 \left(J_{\perp} - \frac{3}{2} \frac{t_{\parallel}^2}{J_{\perp}} + \mu_h \right) \sum_k \sin^2 \frac{\theta_k}{2} \\
&\quad + \frac{3}{2} \frac{t_{\parallel}^2}{J_{\perp} L} \sum_{kk'} \frac{1}{2} \sin \theta_k \sin \theta_{k'} \cos(k - k') + (V + J_{\perp} + 2\mu_h) |\beta|^2 - \mu_h N_h
\end{aligned} \tag{B9}$$

BCS ground state parameter

As a first step, we want to find the stationary point with respect to the BCS coefficient θ_k

$$\begin{aligned}
\frac{\partial \langle \hat{H} \rangle}{\partial \theta_k} &= -2 \frac{t_{\parallel}}{\sqrt{L}} \left[\cos \theta_k \beta \cos(k) + \text{c.c} \right] + \left(t_{\parallel} - \frac{t_{\parallel}}{L} |\beta|^2 \right) \sin \theta_k \cos(k) \\
&\quad + \left(J_{\perp} - \frac{3}{2} \frac{t_{\parallel}^2}{J_{\perp}} + \mu_h \right) \sin \theta_k \\
&\quad + \frac{3}{2} \frac{t_{\parallel}^2}{J_{\perp} L} \sum_{k'} \cos \theta_k \sin \theta_{k'} \cos(k - k') \stackrel{!}{=} 0
\end{aligned} \tag{B10}$$

For simplicity, we define the quantities

$$\begin{aligned}
\xi_k &:= \left(t_{\parallel} - \frac{t_{\parallel}}{L} |\beta|^2 \right) \cos(k) + \left(J_{\perp} - \frac{3}{2} \frac{t_{\parallel}^2}{J_{\perp}} + \mu_h \right) \\
V_{kk'} &:= \frac{3}{2} \frac{t_{\parallel}^2}{J_{\perp}} \cos(k - k')
\end{aligned} \tag{B11}$$

and parametrize θ_k by

$$2v_k u_k = \sin \theta_k = \frac{\Delta_k}{\sqrt{\xi_k^2 + \Delta_k^2}}, \quad u_k^2 - v_k^2 = \cos \theta_k = \frac{\xi_k}{\sqrt{\xi_k^2 + \Delta_k^2}} \tag{B12}$$

From this parametrization, it is straightforward to show that

$$\begin{aligned}
v_k^2 &= \frac{1}{2} \left(1 - \frac{\xi_k}{\sqrt{\xi_k^2 + \Delta_k^2}} \right) \\
u_k^2 &= \frac{1}{2} \left(1 + \frac{\xi_k}{\sqrt{\xi_k^2 + \Delta_k^2}} \right)
\end{aligned} \tag{B13}$$

Substituting into Eq.(B10) yields

$$0 = -2\frac{t_{\parallel}}{\sqrt{L}} \left[\beta \cos(k) + \text{c.c.} \right] + \Delta_k + \frac{1}{L} \sum_{k'} V_{k,k'} \frac{\Delta_{k'}}{\sqrt{\xi_{k'}^2 + \Delta_{k'}^2}} \quad (\text{B14})$$

Finally, we can explicitly write down the *Gap equation* for the BCS state of spinon-chargons

$$\Delta_k = 2\frac{t_{\parallel}}{\sqrt{L}} \left[\beta \cos(k) + \text{c.c.} \right] - \frac{1}{L} \sum_{k'} V_{k,k'} \frac{\Delta_{k'}}{\sqrt{\xi_{k'}^2 + \Delta_{k'}^2}} \quad (\text{B15})$$

BEC ground state parameter

We now compute the stationary point with respect to the BEC parameter β

$$\frac{\partial \langle \hat{H} \rangle}{\partial \beta} = -4\frac{t_{\parallel}}{\sqrt{L}} \sum_k v_k u_k \cos(k) - 4\frac{t_{\parallel}}{L} \beta^* \sum_k \cos(k) |v_k|^2 + (V + J_{\perp} + 2\mu_h) \beta^* \stackrel{!}{=} 0 \quad (\text{B16})$$

By previous considerations $v_k, u_k \in \mathbb{R}$ and $\beta \in \mathbb{C}$. Then, Eq.(B16) can be split by separately considering its imaginary and real parts, which give us, respectively

$$\begin{aligned} \text{Re}(\beta) &= \frac{2\frac{t_{\parallel}}{\sqrt{L}} \sum_k \frac{\Delta_k}{\sqrt{\xi_k^2 + \Delta_k^2}} \cos(k)}{(V + J_{\perp} + 2\mu_h) - 4\frac{t_{\parallel}}{L} \sum_k \frac{1}{2} \left(1 - \frac{\xi_k}{\sqrt{\xi_k^2 + \Delta_k^2}} \right) \cos(k)} \\ \text{Im}(\beta) &= 0 \end{aligned} \quad (\text{B17})$$

where we have expressed the equations in terms of the BCS parameter Δ_k .

Holes number

In Eq. (A13) we have introduced the chemical potential μ_h . This allows us to fix the number of holes in the system by minimizing with respect to μ_h

$$\frac{\partial \langle \hat{H} \rangle}{\partial \mu_h} = 2 \sum_k |v_k|^2 + 2|\beta|^2 - N_h \stackrel{!}{=} 0 \quad (\text{B18})$$

where N_h is the number of holes in the system. Thus, we have an additional equation relating the BEC parameter β and the BCS parameter Δ_k . Explicitly, we have

$$N_h = 2 \sum_k \frac{1}{2} \left(1 - \frac{\xi_k}{\sqrt{\xi_k^2 + \Delta_k^2}} \right) + 2|\beta|^2 \quad (\text{B19})$$

Observables

The energy with respect to the ansatz ground state wave function in Eq. (9) can be expressed in terms of the new parameter Δ_k

$$\begin{aligned} \langle \hat{H} \rangle &= -2\frac{t_{\parallel}}{\sqrt{L}} \sum_k \left[\frac{\Delta_k}{\sqrt{\xi_k^2 + \Delta_k^2}} \beta \cos(k) + \text{c.c.} \right] + 2(t_{\parallel} - 2\frac{t_{\parallel}^2}{L} |\beta|^2) \sum_k \frac{1}{2} \left(1 - \frac{\xi_k}{\sqrt{\xi_k^2 + \Delta_k^2}} \right) \cos(k) \\ &+ 2 \left(J_{\perp} - \frac{3}{2} \frac{t_{\parallel}^2}{J_{\perp}} + \mu_h \right) \sum_k \frac{1}{2} \left(1 - \frac{\xi_k}{\sqrt{\xi_k^2 + \Delta_k^2}} \right) + \frac{3}{4} \frac{t_{\parallel}^2}{J_{\perp} L} \sum_{kk'} \frac{\Delta_k \Delta_{k'}}{\sqrt{\xi_k^2 + \Delta_k^2} \sqrt{\xi_{k'}^2 + \Delta_{k'}^2}} \cos(k - k') \\ &+ (V + J_{\perp} + 2\mu_h) |\beta|^2 - \mu_h N_h \end{aligned} \quad (\text{B20})$$

Moreover, the sc and cc densities are straightforward to obtain $n_f = \frac{2}{L} \sum_k \frac{1}{2} \left(1 - \frac{\xi_k}{\sqrt{\xi_k^2 + \Delta_k^2}} \right)$ and $n_b = \frac{|\beta|^2}{L}$.

Appendix C: Binding energy

For the bilayer model under consideration, the binding energy is defined as

$$E_B(N_h) = 2(E_{N_h-2} - E_{N_h-1}) - (E_{N_h-2} - E_{N_h}) \quad (\text{C1})$$

where N_h is the number of holes in the system, added in an alternating fashion to each layer. In order to compute the binding energy, we consider the BEC limit of the crossover where the holes in the system tend to form tightly bound pairs of chargons. Here, the cc's are described by a non-interacting BEC which is characterized by a vanishing chemical potential $\mu_{\text{BEC}} \simeq 0$. Therefore, the addition to the system of a new bosonic pair (two holes) leaves the ground state energy approximately unchanged: $E_{N_h-2} - E_{N_h} \approx 0$. If only one extra hole is introduced to the system, then it will contribute to the formation of a spinon-chargon with an energy change given by $E_{N_h-1} - E_{N_h} = \Delta_{\text{gap}}$ where Δ_{gap} is the pairing gap emerging from the formation of sc's Cooper pairs.

The binding energy obtained from Eq.(C1) is thus $E_b = 2\Delta_{\text{gap}}$. Here, we briefly discuss how to determine the value of the pairing gap starting from the ansatz wavefunction in Eq.(B1) and focusing on the BCS term $|\Psi\rangle_{\text{BCS}} = \prod_k \left(u_k + v_k \frac{1}{\sqrt{2}} \sum_{\sigma} (-1)^{\sigma} \hat{f}_{k1\sigma}^{\dagger} \hat{f}_{-k0\bar{\sigma}}^{\dagger} \right) |0\rangle$ representing a Gaussian state, which generally is the ground state of a quadratic Hamiltonian. Such Hamiltonian can be expressed using the Nambu spinor formalism

$$\hat{\mathcal{H}} = \sum_k \hat{\psi}_k^{\dagger} (\vec{h}_k \cdot \vec{\sigma}) \hat{\psi}_k \quad (\text{C2})$$

with $\hat{\psi}_k$ the Nambu spinor, $\vec{\sigma} = (\sigma_x, \sigma_y, \sigma_z)$ the Pauli matrices and $\vec{h}_k = (\Delta_k^{(1)}, \Delta_k^{(2)}, \xi_k)$ where $\Delta_k = \Delta_k^{(1)} - i\Delta_k^{(2)}$. Here, the Hamiltonian can be easily diagonalized and the eigenvalues are $\pm E_k = \pm \sqrt{\Delta_k^2 + \xi_k^2}$. Therefore, the energy gap is given by $\Delta_{\text{gap}} = \min_k (E_k)$.

Appendix D: Details of the DMRG simulations

The benchmarks in the main text are obtained using the single-site density matrix renormalization group (DMRG) algorithm implemented in the package SyTen [39, 40]. The implementation of the mixD model is based on the ones in Refs. [30, 41]: We employ $U(1)_{N_{\mu=1}} \otimes U(1)_{N_{\mu=2}} \otimes U(1)_{S_z^{\text{tot}}}$ (with $N_{\mu=i}$ the number of particles in chain i and S_z^{tot} the total magnetization) in the DMRG ground state calculations. This corresponds to charge conservation in each individual leg (since $t_{\perp} = 0$) and total magnetization conservation. As shown in the Appendix of Ref. [41] this makes the ground state search much more efficient compared to calculations with only global charge conservation $U(1)_N \otimes U(1)_{S_z^{\text{tot}}}$. We use bond dimensions up to $\chi = 1024$.